Cerebrovascular damage caused by the gut microbe-derived uraemic toxin *p*-cresol sulfate is prevented by blockade of the epidermal growth factor receptor

Sita N Shah[1], Tobias B-A Knausenberger[1], Emily Connell[2], Gwenaelle Le Gall[2], Tom A. J. Hardy[1], David W. Randall[3,4], Kieran McCafferty[3], Muhammad M. Yaqoob[3,4], E. Solito[4,5], Michael Müller[2], Andrew V. Stachulski[6], Robert C. Glen[7,8], David Vauzour[2], Lesley Hoyles[9] & Simon McArthur[10]*

[1] Blizard Institute, Faculty of Medicine & Dentistry, Queen Mary, University of London, 4, Newark Street, London, UK
[2] Norwich Medical School, Biomedical Research Centre, University of East Anglia, Norwich, UK
[3] Department of Renal Medicine and Transplantation, Royal London Hospital, Barts Health NHS Trust, London, UK
[4] William Harvey Research Institute, Faculty of Medicine & Dentistry, Queen Mary, University of London, John Vane Science Centre, Charterhouse Square, London, UK
[5] Dipartimento di Medicina Molecolare e Biotecnologie Mediche, Università degli Studi di Napoli Federico II, Naples, Italy
[6] Robert Robinson Laboratories, Department of Chemistry, University of Liverpool, Liverpool, UK
[7] Faculty of Medicine, Department of Metabolism, Digestion and Reproduction, Imperial College London, London, UK
[8] Centre for Molecular Informatics, Department of Chemistry, University of Cambridge, Cambridge, UK
[9] Department of Biosciences, School of Science and Technology, Nottingham Trent University, Clifton, Nottingham, UK
[10] Institute of Dentistry, Faculty of Medicine & Dentistry, Queen Mary, University of London, Blizard Institute, 4, Newark Street, London, UK

* Correspondence to Dr Simon McArthur (s.mcarthur@qmul.ac.uk)

Running Title: *p*-cresol sulfate damages the blood-brain barrier

Funding Support
This work was funded by Alzheimer's Research UK Pilot Grant No. ARUK-PPG2016B-6. This project has received funding from the European Union's Horizon 2020 research and innovation programme under grant agreement No 874583. This publication reflects only the authors' views, and the European Commission is not responsible for any use that may be made of the information it contains.

Abstract

Chronic kidney disease is linked to impaired cognitive function and increased neurovascular disease risk even after correction for classical risk factors. The mechanism(s) underlying these links are unclear but may involve interactions of uraemic toxins with the blood-brain barrier (BBB). Here, we studied how the major uraemic toxin *p*-cresol sulfate (pCS) could affect BBB integrity. Exposure of human hCMEC/D3 endothelial cells to pCS dose-dependently increased paracellular permeability and disrupted intercellular tight junctions, a permeabilising effect mirrored in mice. Whole brain RNAseq analysis identified pCS-mediated suppression of neuronal activity, transcription and mitochondrial respiration pathways. *In vitro* studies identified pCS binding to the epidermal growth factor receptor (EGFR), leading *via* annexin A1 and STAT3 signalling to mobilisation of matrix metalloproteinase (MMP)-2/9. Confirming this pathway *in vivo*, the BBB damaging effects of pCS were prevented by pre-treatment with the EGFR antagonist erlotinib or the MMP2/9 inhibitor SB-3CT. Finally, hCMEC/D3 cells exposed to haemodialysis patient serum, but not to that of healthy donors, showed an erlotinib-sensitive increase in paracellular permeability that closely correlated in size to the total serum pCS content. Overall, we define a pathway linking the uraemic toxin pCS with BBB damage suggesting that targeting the EGFR may be useful in mitigating against cerebrovascular damage in chronic kidney disease.

Keywords

Blood-brain barrier, *p*-cresol sulfate, cerebrovascular disease, chronic kidney disease, gut microbiota

Translational Statement

Patients with chronic kidney disease (CKD) have increased risk of cognitive impairment and stroke, pathologies associated cerebromicrovascular disease, but it is not clear why. Here, we show that the uraemic toxin p-cresol sulfate impairs BBB function *in vitro* and *in vivo* through EGFR-dependent MMP mobilisation. Importantly, serum from haemodialysis patients can also impair permeability of an *in vitro* BBB model, an effect prevented by EGFR inhibition, and proportional in magnitude to serum pCS content. Our data suggest that existing EGFR inhibitory drugs might have utility in preventing cerebral small vessel disease in CKD patients.

Abbreviations: BBB, blood–brain barrier; CKD, chronic kidney disease; EGFR, epidermal growth factor receptor; IS, indoxyl sulfate; MMP, matrix metalloproteinase; pCS, *p*-cresol sulfate; pCG, *p*-cresol glucuronide; SPIA, signalling pathway impact analysis; TEER, transendothelial electrical resistance; ZO-1, zonula occludens-1.

Introduction

Communication between the commensal microbiota and host systems is implicated in many areas of health and disease[1]. Substantial evidence highlights gut microbes as modifiers of central nervous system function[2], but far less is known about the mechanism(s) that underlie these links[3]. Microbial modulation of afferent neural[4], immune[5] and neuroendocrine[6] activity has been described, but perhaps the least well characterised route of gut-brain communication is direct exposure to the myriad microbe-derived metabolites present in the circulation[7,8]. We and others have recently shown gut microbe-derived circulating metabolites (e.g. short-chain fatty acids[9,10] and methylamines[11]) to target the blood-brain barrier (BBB), but the impact of other gut microbial metabolites upon the brain vasculature, and their roles in health and disease, are largely unexplored.

One important microbe-derived metabolite given its links with renal dysfunction is *p*-cresol, produced by fermentation of tyrosine and phenylalanine in the colon, particularly by *Coriobacteriaceae* or *Clostridium* species[12]. Luminal *p*-cresol undergoes extensive conjugation in both enterocytes[13] and the liver[14], such that it is found almost exclusively as *p*-cresol sulfate (pCS, ~90 % in humans) and *p*-cresol glucuronide (pCG) in the systemic circulation[15]. Under normal circumstances, both conjugates are efficiently cleared by the kidneys, with an effective plasma half-life of around 30 min in rodents[16]. However, pCS accumulates within the plasma of individuals with compromised renal function[17] and is poorly removed by haemodialysis[18], a feature of importance given that increased plasma concentrations predict mortality in individuals with chronic kidney disease (CKD)[19].

CKD is a complex disorder affecting many aspects of physiology, but is notably associated with significant neurological and cerebrovascular complications[20]. Patients with CKD are at an increased risk of both ischaemic and haemorrhagic stroke, even after correcting for coincident vascular risk factors[21], and tend to have worse functional outcomes post-infarct[22]. Even in the absence of overt stroke, many patients requiring haemodialysis exhibit marked cognitive impairments[23], aspects that together represent major unmet clinical needs[24]. Notably, CKD is associated with both enhanced BBB permeability[25] and the presence of microbleeds[26], both linked with cognitive dysfunction[27,28], suggesting that cerebrovascular damage at least contributes to CKD-associated cognitive disruption.

These links between CKD and cerebrovascular disease, alongside reports from experimental studies showing pCS to induce dermal microvascular leakage[29] and aortic oxidative damage and remodelling[29,30], led us to hypothesise that the gut microbe-host co-metabolite pCS may directly damage the cerebral vasculature, impairing BBB function and contributing to the neurological consequences of CKD. Here, through use of combined *in vitro/in vivo* approaches, we report a clear deleterious effect of pCS upon BBB integrity, mediated through stimulation of the epidermal growth factor receptor (EGFR) and ensuing activation of matrix metalloproteinases (MMPs). Moreover, we establish that antagonism of the EGFR protects against the BBB-permeabilising actions of serum from patients with chronic renal failure, offering a potential new pathway to protect against uraemia-associated cerebrovascular damage linked to the gut-brain-kidney axis.

Methods

Animals

Wild-type male C57Bl/6J mice aged between 7 and 8 weeks (Charles River UK Ltd., Margate, UK) were used for all experiments. All experiments were approved by the QMUL Animal Welfare and Ethical Review Board and were performed in accordance with the ARRIVE guidelines and the UK Animals (Scientific Procedures) Act, 1986, under Project Licence PFA5C4F4F and Personal Licence I6BE7E277. For tissue collection details, see Supplementary Methods.

Human serum samples

Human serum samples were collected from patients undergoing haemodialysis at Barts Health NHS Trust and age-/sex-matched healthy controls who had previously consented for sample inclusion in the Barts Diabetic Kidney Disease Biobank, see Table 2 for demographic details. Ethical approval for the inclusion in the Barts DKC Biobank was provided under REC reference no. 18/EE/0142. Approval for the current study was provided under REC reference no. 20/LO/0361. The study followed established standard operating procedures and all experiments involving human tissue conformed to the principles set out in the World Medical Association Declaration of Helsinki. All serum samples were de-complemented by incubation at 56 °C for 20 min prior to use.

Cell culture

The human cerebromicrovascular endothelial cell line hCMEC/D3 was maintained and treated as described previously[10]. Cells were cultured to confluency in complete endothelial cell growth medium MV2 (PromoCell GmbH, Germany), whereupon VEGF was removed, and cells were further cultured for a minimum of 4 days to enable intercellular tight junction formation prior to experimentation. All cell cultures were used at passages 28-33 to ensure retention of appropriate endothelial characteristics[31].

Analytical protocols

For full details of analytical techniques followed, see Supplementary Methods.

Statistical analysis

Sample sizes were calculated to detect differences of 15 % or more with a power of 0.85 and α set at 5 %, calculations being informed by previously published data[11]. *In vitro* experimental data are expressed as mean ± SEM, with n = 4-9 independent experiments for all studies. Statistical analyses were performed using RStudio 2022.07.1. In all cases, normality of distribution was established using the Shapiro–Wilk test, followed by analysis with two-tailed Student's *t*-tests to compare two groups or, for multiple comparisons, one- or two-way ANOVA with Tukey's HSD *post hoc* test. A *P* value of <5 % was considered significant.

Results

Cresol conjugates exert opposing effects upon BBB integrity

To assess the effects of pCS upon BBB integrity, we first examined its effects upon a simple *in vitro* model of BBB function, namely the paracellular permeability barrier of a monolayer of the immortalised human cerebromicrovascular endothelial line hCMEC/D3[31]. Treatment with pCS (24 h; 10 μM, 100 μM or 1 mM) significantly ($P < 0.05$) and dose-dependently enhanced permeability to a 70 kDa FITC-dextran tracer (Fig. 1A) and reduced transendothelial electrical resistance (TEER; Fig. 1B); notably pCS showed no signs of endothelial toxicity at any concentration tested (Fig. S1). The BBB permeability barrier is underpinned by tight inter-endothelial junctions and their interactions with the actin cytoskeleton; hence, we examined the effect of pCS treatment upon the key tight junction component zonula occludens-1 (ZO-1) and fibrillar actin in hCMEC/D3 monolayers. In comparison with untreated cells, pCS treatment (24 h, 10 μM) markedly disrupted the marginal localisation of ZO-1 (Fig. 1C), as well as disrupting actin fibril arrangement itself (Fig. 1D), with a clear loss of cortical actin and appearance of trans-cytoplasmic fibres.

To confirm that these *in vitro* findings had relevance for whole animal physiology, we treated male C57Bl/6 mice with pCS (10 mg/kg i.p., chosen to approximately double circulating free pCS concentrations[32]; 2 h, 6 h) before assessing BBB permeability through cerebral extravasation of the albumin-binding tracer Evans blue. Treatment of mice with pCS resulted in a significant ($P < 0.02$) increase in brain parenchymal Evans blue at both 2 h and 6 h post-administration (Fig. 1E).

Transcriptomic analyses

To examine potential mechanisms of pCS action, we performed RNAseq analysis of whole-brain transcriptomes, comparing untreated and pCS-treated mice (10 mg/kg i.p., 2 h). We found 380/16,988 genes assayed were significantly differentially expressed ($P < 0.05$, Benjamini-Hochberg): the expression of 91 genes was significantly upregulated in the pCS-treated group, while the expression of 289 was significantly downregulated (Fig. 2A; Table S1). Among BBB-specific genes, the expression of *Slc1a2* ($\log_2$ fold change -1.35), *Adgra2* (1.03) and *Serpini1* (-1.93) was found to be significantly changed ($P < 2.66 \times 10^{-4}$ for all, Benjamini-Hochberg).

Analysis of over-represented Gene Ontology categories within differentially expressed genes using Enrichr[33] revealed that, while no categories associated with significantly up-regulated genes reached statistical significance after multiple testing correction, several biological processes and molecular functions associated with significantly ($P < 0.05$; Benjamini-Hochberg) down-regulated genes could be identified (Fig. 2B). Broadly, these fell into two main categories: ontologies reflective of neuronal function and synaptic activity, and those indicating intracellular protein translocation and metabolism. Signalling Pathway Impact Analysis (SPIA) demonstrated inhibition of pathways associated with glutamatergic synapse, circadian entrainment, and Alzheimer disease (pGFWER < 0.05; Table 1). Topological analysis of the network generated from the 380 significantly differentially expressed genes mapped onto KEGG pathways identified in SPIA (pGFdr < 0.05; Table 1) suggested that the genes for *Prkacb*, *Homer1*, *Tardbp*, *Calm1*, *Calm3*, *Ppp3r1*, *Ppp3cb* and *Grm5* had most control over the network (Fig. 2C; Table S2). Manual curation of SPIA-highlighted genes

identified several broad categories of primarily down-regulated function: neuronal activity, mitochondrial respiration, translation, cell cycle activity, and intracellular Ca^{2+}- and other signalling pathways (Fig. 2C), overall depicting a generalised inhibitory effect of pCS upon brain function.

Permeabilising effects of pCS are mediated through the EGFR

Although transcriptomic analysis did not suggest a clear candidate pathway for the actions of pCS directly upon the cerebral vasculature, previous studies have indicated that it may interact with the EGFR[34], hence we investigated the potential involvement of this receptor in the effects of the metabolite upon the BBB. Initial studies of hCMEC/D3 cells confirmed EGFR expression (Fig. 3A) and showed it to be phosphorylated at Tyr1068 within 15 min of 10 μM pCS stimulation, phosphorylation that was maintained for at least 30 min (Fig. 3B). That this was a direct effect of pCS was confirmed by inclusion of the EGFR-specific inhibitor erlotinib (2.5 μM, 10 min pre-treatment), which effectively prevented EGFR phosphorylation (Fig. 3C).

In light of these interactions, we investigated whether EGFR activation mediated the permeabilising actions of pCS. Pre-treatment with erlotinib (2.5 μM, 10 min pre-treatment) efficiently ablated the pCS-induced (10 μM, 24 h) increase in paracellular permeability (Fig. 3D) and decrease in TEER (Fig. 3E). These functional effects were paralleled by a reduction in pCS-stimulated disruption to the intracellular distribution of the tight junction molecule ZO-1 (Fig. 3F) and to the actin cytoskeleton (Fig. 3G).

While erlotinib has high selectivity for the EGFR, it is not without off-target effects; hence, we confirmed the centrality of this receptor in pCS action through use of targeted siRNA-mediated knockdown. Treatment of hCMEC/D3 cells expressing any of three independent siRNA sequences (knockdown efficiencies of 65.3 %, 56.7 % and 76.8 % respectively, Fig. S2) with pCS (10 μM, 24 h) had little effect on either paracellular permeability (Fig. 3H) or TEER (Fig. 3I). This was in marked contrast to cells that had been either mock transfected or transfected with non-targeting siRNA negative control sequence, in which pCS treatment significantly ($P < 0.05$) increased paracellular permeability (Fig. 3H) and significantly ($P < 0.05$) decreased TEER (Fig. 3I), closely aligning with previous experiments.

pCS stimulation of EGFR activates an ANXA1–STAT3–MMP signalling pathway

EGFR is coupled to a number of intracellular signalling pathways, but one potentially relevant target is the protein annexin A1 (ANXA1)[35], a molecule we have shown to be a major regulator of BBB function[36]. We therefore investigated whether this protein was involved in the response to pCS. Initial experiments confirmed that ANXA1 underwent Tyr21 phosphorylation in response to pCS treatment (10 μM, 30 min; Fig. 4A) in an erlotinib-sensitive manner (2.5 μM, 10 min pre-treatment; Fig. 4B). Using hCMEC/D3 cells stably bearing shRNA sequences to ANXA1[11] (Fig. S3), we further identified that treatment with pCS (10 μM, 24 h) significantly enhanced paracellular permeability in monolayers of wild-type and scramble shRNA-bearing hCMEC/D3 cells, but that this response was notably absent in cells transfected with ANXA1 shRNA sequences (Fig. 4C). Similarly, TEER was significantly ($P < 0.01$) reduced in wild-type and scramble shRNA-bearing hCMEC/D3 cells upon pCS treatment, but not in ANXA1 shRNA transfected cells (Fig. 4D).

Both EGFR signalling and ANXA1 Tyr21 phosphorylation have been linked with the transcription factor STAT3[37,38], hence we examined the impact of pCS treatment upon STAT3

activation. Exposure of hCMEC/D3 cells to pCS (10 μM) significantly ($P < 0.001$) enhanced STAT3 Tyr705 phosphorylation within 15 min (Fig. 4E), an effect that was not seen in cells pre-treated with erlotinib (2.5 μM, 10 min pre-treatment; Fig. 4F) and was attenuated or absent in hCMEC/D3 cells bearing ANXA1 shRNA sequences (Fig. 4G). Notably, pre-treatment of hCMEC/D3 cells with the selective STAT3 inhibitor C188-9 (5 μM, 30 min pre-treatment) significantly ($P \leq 0.002$) reduced the effects of pCS treatment (10 μM, 24 h) upon both paracellular permeability to a 70 kDa FITC-dextran tracer (Fig. 4H) and TEER (Fig. 4I).

Inhibition of MMP activity prevents the permeabilising effects of pCS in vitro

Activation of MMPs, particularly that of MMP-2 and MMP-9, is known to be both downstream of EGFR[34] and STAT3[39] activation, and to be capable of damaging BBB permeability[40], leading us to hypothesise that the permeabilising effects of pCS may be mediated through these enzymes. Stimulation of hCMEC/D3 cells with pCS (10 μM, 24 h) significantly ($P \leq 0.001$) increased MMP-2 and MMP-9 expression (Fig. 5A), a response inhibited by pre-treatment with either the EGFR inhibitor erlotinib (2.5 μM, 10 min pre-treatment) or the STAT3 inhibitor C188-9 (5 μM, 30 min pre-treatment; Fig. 5B). Analysis of hCMEC/D3 conditioned medium by gelatin zymography confirmed that these pCS-induced (10 μM, 24 h) increases in cellular MMP-2 and MMP-9 expression were mirrored by enhanced gelatinase activity (Fig. 5C), an increase again sensitive to erlotinib pre-treatment (2.5 μM, 30 min prior to 10 μM pCS; Fig. 6D).

To judge the relevance of this increase in MMP activity to endothelial barrier integrity, we investigated the effect of selective MMP inhibitors upon the actions of pCS. Pre-treatment of hCMEC/D3 monolayers with either the selective MMP-2 inhibitor ARP 100 (12 nM, 15 min pre-treatment) or the selective MMP-9 inhibitor JNJ0966 (440 nM, 15 min pre-treatment) prevented the disruptive effects of pCS treatment (10 μM, 24 h) upon paracellular permeability to a 70kDa FITC-dextran tracer (Fig. 5E, H), TEER (Fig. 5F, I) and intracellular distribution of the tight junction anchor ZO-1 (Fig. 5G, J).

pCS induces BBB permeability through an EGFR–STAT3–MMP-2/9 pathway in vivo

Having established the EGFR–ANXA1–STAT3–MMP-2/9 pathway as mediating the effects of pCS upon endothelial cell barrier function *in vitro*, we sought to validate this pathway *in vivo*. Accordingly, pre-treatment of male C57Bl/6 mice with the EGFR inhibitor erlotinib (50 mg/kg, i.p., 1 h pre-treatment) prior to pCS injection (10 mg/kg i.p., 2 h; Fig. 6A) suppressed the pCS-induced increase in parenchymal Evans blue tracer extravasation (Fig. 6A), and immunohistochemical appearance of Tyr21 phospho-ANXA1 (Fig. S4), MMP-2 and MMP-9 (Fig. 6C) within the cerebrovascular wall. Confirming the importance of pCS-induced MMP-2/9 activity in mediating BBB disruption, pre-treatment of mice with the MMP-2/9 dual-specific inhibitor SB-3CT (10 mg/kg i.p., 1 h pre-treatment) also prevented pCS-induced (10 mg/kg i.p., 2h) Evans blue extravasation (Fig. 6B), and ameliorated pCS-induced disruption of vascular ZO-1 expression (Fig. 6D).

Treatment with the EGFR inhibitor erlotinib can prevent the permeabilising effect of CKD patient serum upon hCMEC/D3 monolayers

While renal failure is associated with damage to the cerebral vasculature, it is also associated with altered circulating levels of numerous potential uraemic toxins, of which pCS is only one example, albeit an important one. Most notably, the EGFR has been demonstrated to interact with the gut microbe-derived uraemic toxin indoxyl sulfate (IS)[41], although this metabolite did

not affect paracellular permeability to a 70 kDa FITC-dextran tracer or the TEER of hCMEC/D3 monolayers at any concentration tested (5 μM, 25 μM, 50 μM; Fig. S5).

To investigate the relative importance of pCS in mediating the cerebrovascular symptoms of CKD, we exposed hCMEC/D3 monolayers for 24 h to medium containing 20 % de-complemented serum from individuals undergoing haemodialysis for nephropathy or age-matched healthy donors (full donor details in Table 2), alone or in combination with erlotinib (2.5 μM, 10 min pre-treatment). Treatment of hCMEC/D3 cells with haemodialysis patient sera, but not with that from healthy donors, significantly (P = 0.004) enhanced paracellular permeability to a 70 kDa FITC-dextran tracer, an effect reversed by erlotinib pre-treatment (Fig. 7A). Interestingly, however, neither exposure of hCMEC/D3 cells to healthy donor nor to haemodialysis patient sera affected TEER, with or without erlotinib pre-incubation (Fig. 7B). Moreover, similar treatment of hCMEC/D3 cells with sera from haemodialysis patients, but again not with that from healthy donors, significantly (P < 0.05) increased expression of MMP-2 (Fig. 7C) and MMP-9 (Fig. 7D).

Having established that sera from individuals with renal failure could modulate permeability of our *in vitro* BBB model in an erlotinib-sensitive manner, we examined the relative contributions of different amino acid-derived potential uraemic toxins to this response. Following analysis of serum levels of different metabolites by LC-MS/MS (Table 3), we correlated serum concentrations with changes in paracellular permeability; only correlations with pCS (rho = 0.675, P_{FDR} = 0.01; Fig. 7E) or the tryptophan metabolite xanthurenic acid (rho = 0.442, P_{FDR} = 0.02; Fig. 7F) remained significant following correction for multiple testing.

Discussion

Impaired kidney function has serious consequences for virtually every organ system in the body, and the central nervous system is no exception. Patients with CKD, including those at not yet requiring dialysis, exhibit significant cognitive decline[42] and enhanced stroke risk[43,44], even after correction for typical cardiovascular risk factors. Cerebral microvascular disease and BBB disruption are thought to underlie these links[45], but little is known about how renal impairment results in BBB damage. Here we present data indicating a novel BBB-disruptive role for the major uraemic toxin pCS, acting *via* the EGFR to mobilise MMP activity. Moreover, we show that pCS treatment induces widespread transcriptomic changes within the brain, rapidly dampening numerous aspects of neuronal activity and metabolism. Together, these data strongly implicate pCS as a major contributory factor to the links between kidney failure and impaired brain function.

Interactions of pCS with the peripheral vasculature have previously been reported, with evidence of arterial leakage in patients with CKD[46,47] and in animal[29] and *in vitro* models of uraemia[46,47]. Mechanistically, very high levels of pCS can cause inter-endothelial adherens junction disruption[46,47], potentially underlying uraemia-associated endothelial leakage. Here, we extend the damaging actions of pCS to the cerebral vasculature and BBB *in vivo*, acting at concentrations similar to those of free pCS seen at stages III-IV of CKD[48]. We further provide mechanistic evidence coupling pCS agonism at the EGFR, *via* phosphorylation of ANXA1 and STAT3 to mobilisation of MMP-2 and -9. Importantly, these actions appear clinically relevant, with the serum of human patients undergoing haemodialysis impairing the permeability barrier of an *in vitro* BBB model with a potency highly correlated to serum levels of pCS, an effect prevented by co-administration of the EGFR antagonist erlotinib. Future studies will be required to investigate the potential of targeting the EGFR as a risk-reduction strategy for cerebrovascular complications in CKD, an aspect currently only addressed through clinical management of hypertension.

Cerebral small vessel disease, for which BBB failure is a fundamental driver[49], is thought to contribute to both the cognitive impairments and enhanced stroke risk seen in CKD patients[50,51]. What is less clear, partly due to the obscuring effects of the relationship between CKD and cerebrovascular risk factors such as diabetes and hypertension, is why this is the case. Notably, activation of MMPs within the neurovascular unit has been reported in several forms of cerebrovascular disease, including stroke[52] and traumatic injury[53], and especially cerebral small vessel disease[54,55]. By identifying a mechanistic link between pCS, cerebrovascular MMP activity and impaired BBB integrity, we provide an explanation for how CKD might damage cerebral vessels. Moreover, whilst local MMP activity has been demonstrated in a range of kidney disorders[56], whether this holds true in the brains of CKD patients is unknown. Our data indicating both a close correlation between pCS content and the BBB-permeabilising actions of haemodialysis patient serum, and moreover that exposure to such serum directly enhances endothelial MMP expression, suggests that this is highly likely.

While enhanced BBB permeability is a recognised driver of damage to cognitive function[57], our data suggest that the effects of pCS upon brain function extend beyond its immediate impact on the cerebral vasculature. Transcriptional analysis of pCS-treated mice indicates a more generalised inhibitory effect of the toxin upon neural activity, which may also be expected

to impair cognitive abilities. Further analysis will be needed to explore this aspect of pCS action, but it does align with previous studies linking pCS and impaired cognition in humans[58] and mice[59,60]. Our description of the EGFR as a major mediator of pCS actions in the brain may point to potential therapeutic strategies; several EGFR inhibitors (e.g., erlotinib, gefitinib) and monoclonal antibodies (e.g., cetuximab, necitumumab) are currently licenced for clinical use, suggesting there may be scope for broader use in CKD.

Intriguingly, while pCS clearly influenced BBB permeability, we found no evidence that this was true for the other major uraemic toxin, IS. This is perhaps surprising, given previous evidence that IS concentrations correlate with BBB impairment in partially nephrectomised rats[61] and vascular disease in CKD patients[62]. It should be noted, however, that reversal of the nephrectomy-induced rise in serum IS by treatment with the oral intestinal sorbent AST-120 did not improve BBB permeability measures[61], suggesting that agents other than solely IS may be responsible for cerebrovascular barrier impairment following nephrectomy. Taken alongside our recent demonstration that the CKD-associated molecule trimethylamine *N*-oxide (TMAO) exerted marked beneficial effects upon both the BBB and cognition at levels seen in metabolically healthy individuals[11], it appears the generalised assumption that uraemia-associated molecules are always deleterious may need revisiting[63].

While pCS predominates in the circulation, it is not the only *p*-cresol conjugate found in blood, with pCG representing a significant, albeit minor, fraction[15]. Moreover, levels of pCG do increase markedly with worsening CKD stages, and have been shown to correlate with mortality risk in a similar way to pCS[64]. However, we have shown pCG to exert very different actions upon the BBB to pCS, with its administration at physiologically relevant levels *in vivo* enhancing barrier integrity by antagonism of basal circulating lipopolysaccharide interactions with TLR4[65]. Moreover, whole brain RNAseq analysis of pCG-treated mice indicated a positive regulation in neuronal activity gene ontologies, notably opposite to the suppressive effects of pCS described here[65]. That the two major conjugates of gut microbe-derived *p*-cresol should so markedly differ in effect upon the brain is striking, emphasising the need for mechanistic studies of uraemic toxin actions before drawing conclusions about their clinical role.

Most circulating pCS is ultimately derived by the actions of gut microbes upon dietary amino acids[66], thus our description of its effects upon the BBB further emphasises the importance of this facet of the gut-brain-kidney axis. Notably, while we and others have other gut microbe-derived metabolites, including short-chain fatty acids[9,10], methylamines[11], and pCG[65] to reinforce BBB integrity in healthy animals, pCS is overtly detrimental in its effects. Given the wide range of metabolites produced by gut microbes, that some agents are deleterious at supraphysiological concentrations is unsurprising but does emphasise the importance of mechanistic analyses of gut-brain communication pathways. Overall, our description of pCS as a major link between gut microbes, kidney function and the cerebral vasculature highlights the role of the gut microbiota in at least some of the systemic effects of renal disease, emphasising its potential as a therapeutic target for clinical management of CKD.

Author Contributions

SNS, TBAK, TAJH and SM performed cellular assays and *in vivo*/*ex vivo* analyses. EC, GLG, MM and DV performed LC-MS/MS analysis. DWR, KM and MMY provided human serum samples. ES produced and provided shRNA treated hCMEC/D3 clones. LH undertook all processing and analyses of transcriptomic data. RCG and AVS provided critically valuable insight and advice throughout the project. SM conceptualised the study, designed the experiments and wrote the manuscript. All authors read and approved the final version of the manuscript.

Supplementary Material

Supplementary Methods
Figure S1: Exposure of hCMEC/D3 cells to pCS does not affect cell viability
Figure S2: Suppression of cell surface EGFR expression in hCMEC/D3 cells can be successfully achieved using siRNA
Figure S3: Stable transfection of hCMEC/D3 cells with shRNA sequences targeting ANXA1 causes a reduction in protein expression
Figure S4: *In vivo* treatment with pCS stimulates Tyr21 phosphorylation of ANXA1 in an erlotinib-sensitive manner
Figure S5: Treatment of hCMEC/D3 cells with indoxyl sulfate (IS) does not affect endothelial barrier functions at physiological or uraemia-associated concentrations
Table S1: Outputs from DESeq2 analysis of differentially expressed genes
Table S2: Summary network statistics for transcriptomic data mapped to KEGG pathways

References

1. Marchesi JR, Adams DH, Fava F, et al. The gut microbiota and host health: a new clinical frontier. *Gut*. 2016;65(2):330–339.
2. Sarkar A, Harty S, Lehto SM, et al. The Microbiome in Psychology and Cognitive Neuroscience. *Trends Cogn. Sci.* 2018;22(7):611–636.
3. Chakrabarti A, Geurts L, Hoyles L, et al. The microbiota-gut-brain axis: pathways to better brain health. Perspectives on what we know, what we need to investigate and how to put knowledge into practice. *Cell. Mol. Life Sci. CMLS*. 2022;79(2):80.
4. Forsythe P, Bienenstock J, Kunze WA. Vagal pathways for microbiome-brain-gut axis communication. *Adv. Exp. Med. Biol.* 2014;817:115–133.
5. Powell N, Walker MM, Talley NJ. The mucosal immune system: master regulator of bidirectional gut-brain communications. *Nat. Rev. Gastroenterol. Hepatol.* 2017;14(3):143–159.
6. Cani PD, Knauf C. How gut microbes talk to organs: The role of endocrine and nervous routes. *Mol. Metab.* 2016;5(9):743–752.
7. Wikoff WR, Anfora AT, Liu J, et al. Metabolomics analysis reveals large effects of gut microflora on mammalian blood metabolites. *Proc. Natl. Acad. Sci. U. S. A.* 2009;106(10):3698–3703.
8. Connell E, Le Gall G, Pontifex MG, et al. Microbial-derived metabolites as a risk factor of age-related cognitive decline and dementia. *Mol. Neurodegener.* 2022;17(1):43.
9. Braniste V, Al-Asmakh M, Kowal C, et al. The gut microbiota influences blood-brain barrier permeability in mice. *Sci. Transl. Med.* 2014;6(263):263ra158.
10. Hoyles L, Snelling T, Umlai U-K, et al. Microbiome-host systems interactions: protective effects of propionate upon the blood-brain barrier. *Microbiome*. 2018;6(1):55.
11. Hoyles L, Pontifex MG, Rodriguez-Ramiro I, et al. Regulation of blood-brain barrier integrity by microbiome-associated methylamines and cognition by trimethylamine N-oxide. *Microbiome*. 2021;9(1):235.
12. Saito Y, Sato T, Nomoto K, Tsuji H. Identification of phenol- and p-cresol-producing intestinal bacteria by using media supplemented with tyrosine and its metabolites. *FEMS Microbiol. Ecol.* 2018;94(9):.
13. Ramakrishna BS, Gee D, Weiss A, et al. Estimation of phenolic conjugation by colonic mucosa. *J. Clin. Pathol.* 1989;42(6):620–623.
14. Rong Y, Kiang TKL. Characterizations of Human UDP-Glucuronosyltransferase Enzymes in the Conjugation of p-Cresol. *Toxicol. Sci. Off. J. Soc. Toxicol.* 2020;176(2):285–296.
15. Gryp T, Vanholder R, Vaneechoutte M, Glorieux G. p-Cresyl Sulfate. *Toxins*. 2017;9(2):.
16. Ni J, Zhang W, Zhu Z, et al. In vivo kinetics of the uremic toxin p-cresyl sulfate in mice with variable renal function. *Ther. Apher. Dial. Off. Peer-Rev. J. Int. Soc. Apher. Jpn. Soc. Apher. Jpn. Soc. Dial. Ther.* 2014;18(6):637–642.
17. Meert N, Schepers E, Glorieux G, et al. Novel method for simultaneous determination of p-cresylsulphate and p-cresylglucuronide: clinical data and pathophysiological implications. *Nephrol. Dial. Transplant. Off. Publ. Eur. Dial. Transpl. Assoc. - Eur. Ren. Assoc.* 2012;27(6):2388–2396.
18. Sirich TL. Obstacles to reducing plasma levels of uremic solutes by hemodialysis. *Semin. Dial.* 2017;30(5):403–408.
19. Liabeuf S, Barreto DV, Barreto FC, et al. Free p-cresylsulphate is a predictor of mortality in patients at different stages of chronic kidney disease. *Nephrol. Dial. Transplant. Off. Publ. Eur. Dial. Transpl. Assoc. - Eur. Ren. Assoc.* 2010;25(4):1183–1191.
20. Weiner DE, Gaussoin SA, Nord J, et al. Cognitive Function and Kidney Disease: Baseline Data From the Systolic Blood Pressure Intervention Trial (SPRINT). *Am. J. Kidney Dis. Off. J. Natl. Kidney Found.* 2017;70(3):357–367.
21. Ghoshal S, Freedman BI. Mechanisms of Stroke in Patients with Chronic Kidney Disease. *Am. J. Nephrol.* 2019;50(4):229–239.

22. El Husseini N, Fonarow GC, Smith EE, et al. Renal Dysfunction Is Associated With Poststroke Discharge Disposition and In-Hospital Mortality: Findings From Get With The Guidelines-Stroke. *Stroke*. 2017;48(2):327–334.
23. Nulsen RS, Yaqoob MM, Mahon A, et al. Prevalence of cognitive impairment in patients attending pre-dialysis clinic. *J. Ren. Care*. 2008;34(3):121–126.
24. O'Lone E, Howell M, Viecelli AK, et al. Identifying critically important cardiovascular outcomes for trials in hemodialysis: an international survey with patients, caregivers and health professionals. *Nephrol. Dial. Transplant.* 2020;35(10):1761–1769.
25. Lau WL, Nunes ACF, Vasilevko V, et al. Chronic Kidney Disease Increases Cerebral Microbleeds in Mouse and Man. *Transl. Stroke Res.* 2019;
26. Chai C, Wang Z, Fan L, et al. Increased Number and Distribution of Cerebral Microbleeds Is a Risk Factor for Cognitive Dysfunction in Hemodialysis Patients: A Longitudinal Study. *Medicine (Baltimore)*. 2016;95(12):e2974.
27. Montagne A, Barnes SR, Sweeney MD, et al. Blood-brain barrier breakdown in the aging human hippocampus. *Neuron*. 2015;85(2):296–302.
28. Taheri S, Gasparovic C, Huisa BN, et al. Blood-brain barrier permeability abnormalities in vascular cognitive impairment. *Stroke J. Cereb. Circ.* 2011;42(8):2158–63.
29. Tang W-H, Wang C-P, Yu T-H, et al. Protein-bounded uremic toxin p-cresylsulfate induces vascular permeability alternations. *Histochem. Cell Biol.* 2018;149(6):607–617.
30. Gross P, Massy ZA, Henaut L, et al. Para-cresyl sulfate acutely impairs vascular reactivity and induces vascular remodeling. *J. Cell. Physiol.* 2015;230(12):2927–2935.
31. Weksler B, Romero IA, Couraud P-O. The hCMEC/D3 cell line as a model of the human blood brain barrier. *Fluids Barriers CNS*. 2013;10(1):16.
32. Koppe L, Alix PM, Croze ML, et al. p-Cresyl glucuronide is a major metabolite of p-cresol in mouse: in contrast to p-cresyl sulphate, p-cresyl glucuronide fails to promote insulin resistance. *Nephrol. Dial. Transplant.* 2017;32(12):2000–2009.
33. Xie Z, Bailey A, Kuleshov MV, et al. Gene Set Knowledge Discovery with Enrichr. *Curr. Protoc.* 2021;1(3):e90.
34. Sun C-Y, Young G-H, Hsieh Y-T, et al. Protein-bound uremic toxins induce tissue remodeling by targeting the EGF receptor. *J. Am. Soc. Nephrol. JASN*. 2015;26(2):281–290.
35. Futter CE, Felder S, Schlessinger J, Ullrich A, Hopkins CR. Annexin I is phosphorylated in the multivesicular body during the processing of the epidermal growth factor receptor. *J. Cell Biol.* 1993;120(1):77–83.
36. Cristante E, McArthur S, Mauro C, et al. Identification of an essential endogenous regulator of blood-brain barrier integrity, and its pathological and therapeutic implications. *Proc. Natl. Acad. Sci. U. S. A.* 2013;110(3):832–841.
37. Colamatteo A, Maggioli E, Azevedo Loiola R, et al. Reduced Annexin A1 Expression Associates with Disease Severity and Inflammation in Multiple Sclerosis Patients. *J. Immunol. Baltim. Md 1950*. 2019;203(7):1753–1765.
38. Erdogan F, Radu TB, Orlova A, et al. JAK-STAT core cancer pathway: An integrative cancer interactome analysis. *J. Cell. Mol. Med.* 2022;26(7):2049–2062.
39. Xie T-X, Wei D, Liu M, et al. Stat3 activation regulates the expression of matrix metalloproteinase-2 and tumor invasion and metastasis. *Oncogene*. 2004;23(20):3550–3560.
40. Rempe RG, Hartz AMS, Bauer B. Matrix metalloproteinases in the brain and blood-brain barrier: Versatile breakers and makers. *J. Cereb. Blood Flow Metab. Off. J. Int. Soc. Cereb. Blood Flow Metab.* 2016;36(9):1481–1507.
41. Jansen J, Jansen K, Neven E, et al. Remote sensing and signaling in kidney proximal tubules stimulates gut microbiome-derived organic anion secretion. *Proc. Natl. Acad. Sci. U. S. A.* 2019;116(32):16105–16110.
42. Murray AM, Bell EJ, Tupper DE, et al. The Brain in Kidney Disease (BRINK) Cohort Study: Design and Baseline Cognitive Function. *Am. J. Kidney Dis. Off. J. Natl. Kidney Found.* 2016;67(4):593–600.

43. Wakasugi M, Yokoseki A, Wada M, et al. Stroke incidence and chronic kidney disease: A hospital-based prospective cohort study. *Nephrol. Carlton Vic*. 2022;27(7):577–587.
44. Chronic Kidney Disease Prognosis Consortium, Matsushita K, van der Velde M, et al. Association of estimated glomerular filtration rate and albuminuria with all-cause and cardiovascular mortality in general population cohorts: a collaborative meta-analysis. *Lancet Lond. Engl.* 2010;375(9731):2073–2081.
45. Toyoda K. Cerebral small vessel disease and chronic kidney disease. *J. Stroke*. 2015;17(1):31–37.
46. Chen S-C, Huang S-Y, Wu C-C, Hsu C-F. P-Cresylsulfate, the Protein-Bound Uremic Toxin, Increased Endothelial Permeability Partly Mediated by Src-Induced Phosphorylation of VE-Cadherin. *Toxins*. 2020;12(2):E62.
47. Maciel RAP, Cunha RS, Busato V, et al. Uremia Impacts VE-Cadherin and ZO-1 Expression in Human Endothelial Cell-to-Cell Junctions. *Toxins*. 2018;10(10):E404.
48. Rossi M, Campbell K, Johnson D, et al. Uraemic toxins and cardiovascular disease across the chronic kidney disease spectrum: an observational study. *Nutr. Metab. Cardiovasc. Dis. NMCD*. 2014;24(9):1035–1042.
49. Wardlaw JM, Makin SJ, Valdés Hernández MC, et al. Blood-brain barrier failure as a core mechanism in cerebral small vessel disease and dementia: evidence from a cohort study. *Alzheimers Dement.* 2017;13(6):634–643.
50. Lau WL, Huisa BN, Fisher M. The Cerebrovascular-Chronic Kidney Disease Connection: Perspectives and Mechanisms. *Transl. Stroke Res.* 2017;8(1):67–76.
51. Vinters HV, Magaki SD, Williams CK. Neuropathologic Findings in Chronic Kidney Disease (CKD). *J. Stroke Cerebrovasc. Dis. Off. J. Natl. Stroke Assoc.* 2021;30(9):105657.
52. Rosell A, Ortega-Aznar A, Alvarez-Sabín J, et al. Increased brain expression of matrix metalloproteinase-9 after ischemic and hemorrhagic human stroke. *Stroke*. 2006;37(6):.
53. Muradashvili N, Benton RL, Saatman KE, Tyagi SC, Lominadze D. Ablation of matrix metalloproteinase-9 gene decreases cerebrovascular permeability and fibrinogen deposition post traumatic brain injury in mice. *Metab. Brain Dis.* 2015;30(2):411–426.
54. Adair JC, Charlie J, Dencoff JE, et al. Measurement of gelatinase B (MMP-9) in the cerebrospinal fluid of patients with vascular dementia and Alzheimer disease. *Stroke*. 2004;35(6):e159-162.
55. Zhao J, Li Q, Meng L, et al. Relationship between MMP-9 serum levels and tHcy levels and total imaging load and cognitive dysfunction. *J. Stroke Cerebrovasc. Dis. Off. J. Natl. Stroke Assoc.* 2022;31(12):106759.
56. Zakiyanov O, Kalousová M, Zima T, Tesař V. Matrix metalloproteinases and tissue inhibitors of matrix metalloproteinases in kidney disease. *Adv. Clin. Chem.* 2021;105:141–212.
57. Nation DA, Sweeney MD, Montagne A, et al. Blood-brain barrier breakdown is an early biomarker of human cognitive dysfunction. *Nat. Med.* 2019;25(2):270–276.
58. Wang Y, Nong Y, Zhang X, et al. Comparative plasma metabolomic analysis to identify biomarkers for lead-induced cognitive impairment. *Chem. Biol. Interact.* 2022;366:110143.
59. Sun C-Y, Li J-R, Wang Y-Y, et al. p-Cresol Sulfate Caused Behavior Disorders and Neurodegeneration in Mice with Unilateral Nephrectomy Involving Oxidative Stress and Neuroinflammation. *Int. J. Mol. Sci.* 2020;21(18):E6687.
60. Sato E, Saigusa D, Mishima E, et al. Impact of the Oral Adsorbent AST-120 on Organ-Specific Accumulation of Uremic Toxins: LC-MS/MS and MS Imaging Techniques. *Toxins*. 2017;10(1):E19.
61. Bobot M, Thomas L, Moyon A, et al. Uremic Toxic Blood-Brain Barrier Disruption Mediated by AhR Activation Leads to Cognitive Impairment during Experimental Renal Dysfunction. *J. Am. Soc. Nephrol. JASN*. 2020;31(7):1509–1521.
62. Barreto FC, Barreto DV, Liabeuf S, et al. Serum indoxyl sulfate is associated with vascular disease and mortality in chronic kidney disease patients. *Clin. J. Am. Soc. Nephrol. CJASN*. 2009;4(10):1551–1558.

63. Vanholder R, Nigam SK, Burtey S, Glorieux G. What If Not All Metabolites from the Uremic Toxin Generating Pathways Are Toxic? A Hypothesis. *Toxins*. 2022;14(3):221.
64. Liabeuf S, Glorieux G, Lenglet A, et al. Does p-cresylglucuronide have the same impact on mortality as other protein-bound uremic toxins? *PloS One*. 2013;8(6):e67168.
65. Stachulski AV, Knausenberger TB-A, Shah SN, Hoyles L, McArthur S. A host-gut microbial amino acid co-metabolite, p-cresol glucuronide, promotes blood-brain barrier integrity in vivo. *Tissue Barriers*. 2022;2073175.
66. Saito Y, Sato T, Nomoto K, Tsuji H. Identification of phenol- and p-cresol-producing intestinal bacteria by using media supplemented with tyrosine and its metabolites. *FEMS Microbiol. Ecol.* 2018;94(9):125.

Figure Legends

Figure 1: Exposure to pCS increases permeability of human cerebromicrovascular endothelial cells *in vitro* and the murine BBB *in vivo*. a) Incubation of hCMEC/D3 cell monolayers with pCS (10 μM, 100 μM, 1 mM; 24 h) dose-dependently increased paracellular permeability to a 70 kDa FITC-dextran conjugate; data are mean ± s.e.m., n = 9 independent experiments. b) Incubation of hCMEC/D3 cell monolayers with pCS (10 μM, 100 μM, 1 mM; 24 h) dose-dependently reduced TEER; data are mean ± s.e.m., n = 9 independent experiments. c, d) Confocal microscopic analysis of expression of c) AF488-phalloidin labelled actin filaments (white) or d) the tight junction component zona occludens-1 (ZO-1; white) in hCMEC/D3 cells following treatment for 24 h with 10 μM pCS, nuclei are counterstained with DAPI (blue), scale = 15 μm. Images are representative of at least three independent experiments. e) Treatment of male C57Bl/6 mice by i.p. injection of pCS (10 mg/kg) caused a time-dependent increase in extravasation of Evans blue tracer into the CNS parenchyma, reaching statistical significance at both 2 h and 6 h post administration; data are mean ± s.e.m., n = 5-6 animals.

Figure 2: Exposure of mice to pCS for 2 h significantly affects brain gene expression. a) Volcano plot showing the 380 significantly differentially expressed genes among the 16,988 mouse genes examined in this study (n = 5 animals per group (treated, negative control)). Black data points: no significant change in expression; red dots, significantly ($P < 0.05$, Benjamini-Hochberg) upregulated expression in the pCS group compared with the negative control; blue dots, significantly ($P < 0.05$, Benjamini-Hochberg) downregulated expression in the pCS group compared with the negative control; n=5 per group. b) Biological processes (above) and molecular functions (below) of genes found to be significantly downregulated (n= 289) upon exposure of mice to pCS, based on Enrichr *P* value ranking from Gene Ontology analysis. c) Topological analysis of the KEGG network resulting from mapping the 380 significantly ($P < 0.05$, Benjamini-Hochberg) differentially expressed genes onto the 17 KEGG *Mus musculus* metabolic pathways listed in Table 1. Blue solid circles, genes whose expression is significantly downregulated in the pCS group compared with the control; red solid circles, genes whose expression is significantly upregulated in the pCS group compared with the control. Thick outline colours around the solid circles correspond to the molecular functions listed in the legend. Network summary statistics are available in Table S2.

Figure 3: pCS regulates cerebromicrovascular cell permeability *in vitro* through activation of the EGFR. a) Stimulation of hCMEC/D3 cells with pCS (24 h, 10 μM) has no effect on cell surface expression of EGFR; data are mean ± s.e.m., n = 4 independent experiments; representative flow cytometry histograms are shown. b) Treatment of hCMEC/D3 cells with pCS (10 μM) causes a time-dependent increase in EGFR Tyr1068 phosphorylation, maintained for at least 30 min; data are mean ± s.e.m., n = 9 independent experiments; representative flow cytometry histograms are shown. c) Pre-treatment of hCMEC/D3 cells with erlotinib (2.5 μM, 10 min) prevents EGFR Tyr1068 phosphorylation in response to pCS treatment (10 μM, 30 min), data are mean ± s.e.m., n = 6 independent experiments; representative flow cytometry histograms are shown. d) Pre-treatment of hCMEC/D3 cell monolayers with erlotinib (2.5 μM, 10 min) prevents the increase in paracellular permeability to a 70 kDa FITC-dextran conjugate induced by pCS stimulation (10 μM, 24 h); data are mean ± s.e.m., n = 9 independent experiments. e) Pre-treatment of hCMEC/D3 cell monolayers with erlotinib (2.5 μM, 10 min) prevents the reduction in TEER

induced by pCS stimulation (10 μM, 24 h); data are mean ± s.e.m., n = 9 independent experiments. f) Confocal microscopic analysis of expression of the tight junction component zona occludens-1 (ZO-1; white) in hCMEC/D3 cells following treatment with either pCS (10 μM, 24 h), erlotinib (2.5 μM, 24 h) or both (erlotinib 2.5 μM, 10 min pre-treatment, followed by pCS 10 μM, 24 h); nuclei are counterstained with DAPI (blue), scale bar = 15 μm. Images are representative of at least three independent experiments. g) Confocal microscopic analysis of expression of AF488-conjugated phalloidin labelled actin filaments (white) in hCMEC/D3 cells following treatment with either pCS (10 μM, 24 h), erlotinib (2.5 μM, 24 h) or both (erlotinib 2.5 μM, 10 min pre-treatment, followed by pCS 10 μM, 24 h); nuclei are counterstained with DAPI (blue), scale bar = 15 μm. Images are representative of at least three independent experiments. h) Paracellular permeability to a 70 kDa FITC-dextran conjugate of hCMEC/D3 cell monolayers bearing siRNA sequences targeting the EGFR (siRNA 5, siRNA 11, siRNA 12), a non-targeting negative control siRNA sequence, or that had been mock transfected, with or without stimulation with pCS (10 μM, 24 h); data are mean ± s.e.m., n = 4 independent experiments. i) TEER of hCMEC/D3 cell monolayers bearing siRNA sequences targeting the EGFR (siRNA 5, siRNA 11, siRNA 12), a non-targeting negative control siRNA sequence, or that had been mock transfected, with or without stimulation with pCS (10 μM, 24 h); data are mean ± s.e.m., n = 3 independent experiments.

Figure 4: Stimulation of EGFR by pCS activates a downstream ANXA1–STAT3 signalling pathway. a) Stimulation of hCMEC/D3 cells with pCS (10 μM, 30 min) increases the ratio of Tyr21 phosphorylated to total annexin A1; data are mean ± s.e.m., n = 7 independent experiments; representative flow cytometry histograms are shown. b) Pre-treatment of hCMEC/D3 cells with erlotinib (2.5 μM, 10 min) prevents the increase in the Tyr21 phosphorylated to total ANXA1 expression ratio induced by pCS stimulation (10 μM, 30 min); data are mean ± s.e.m., n = 6 independent experiments. c) Paracellular permeability to a 70 kDa FITC-dextran tracer of monolayers of wild-type hCMEC/D3 cells, or hCMEC/D3 cells stably transfected with either a scramble shRNA sequence or one of three independent shRNA sequences targeting ANXA1 following stimulation with pCS (10 μM, 24 h); data are mean ± s.e.m., *n* = 4 independent experiments. d) TEER of monolayers of wild-type hCMEC/D3 cells, or hCMEC/D3 cells stably transfected with either a scramble shRNA sequence or one of three independent shRNA sequences targeting ANXA1 following stimulation with pCS (10 μM, 24 h); data are mean ± s.e.m., *n* = 4 independent experiments. e) Stimulation of hCMEC/D3 cells with pCS (10 μM) causes a time-dependent increase in expression of Tyr705 phosphorylated STAT3; data are mean ± s.e.m., n = 7 independent experiments; representative flow cytometry histograms are shown. f) Pre-treatment of hCMEC/D3 cells with erlotinib (2.5 μM, 10 min) prevents the increase in Tyr705 phosphorylated STAT3 expression induced by pCS treatment (10 μM, 30 min); data are mean ± s.e.m., n = 6 independent experiments. g) Expression of Tyr705 phosphorylated STAT3 in wild-type hCMEC/D3 cells, or hCMEC/D3 cells stably transfected with either a scramble shRNA sequence or one of three independent shRNA sequences targeting ANXA1 following stimulation with pCS (10 μM), expressed as percentage of untreated cells; data are mean ± s.e.m., n = 4 independent experiments. h) Pre-treatment of hCMEC/D3 cell monolayers with the STAT3 inhibitor C188-9 (5 μM, 30 min) prevents the increase in paracellular permeability to a 70 kDa FITC-dextran conjugate induced by pCS stimulation (10 μM, 24 h); data are mean ± s.e.m., n = 6 independent experiments. i) Pre-treatment of hCMEC/D3 cell monolayers with C188-9 (5 μM, 30 min) prevents the reduction in TEER induced by pCS stimulation (10 μM, 24 h); data are mean ± s.e.m., n = 6 independent experiments.

Figure 5: pCS enhances endothelial permeability *via* mobilisation of active MMP2 and MMP9. a) Treatment of hCMEC/D3 cells with pCS (10 μM, 24 h) increases expression of MMP2 and MMP9; data are mean ± s.e.m., n = 7 independent experiments. b) Stimulation of MMP2 or MMP9 expression in hCMEC/D3 cells by pCS (10 μM, 24 h) is prevented by either erlotinib (2.5 μM, 10 min pre-treatment) or C188-9 (5 μM, 30 min pre-treatment); data are mean ± s.e.m., n = 6 independent experiments. c) Active MMP2 and MMP9 are secreted into the culture medium of hCMEC/D3 cells in response to pCS (10 μM, 24 h) stimulation; data are mean ± s.e.m., n = 6 independent experiments; a typical gelatin zymography is shown, highlighting both active MMP2 and MMP9 and artifactually revealed pro-MMP2 and pro-MMP9 activity. d) Active MMP2 and MMP9 release from hCMEC/D3 cells into culture medium in response to pCS (10 μM, 24 h) stimulation is prevented by erlotinib (2.5 μM, 10 min pre-treatment); data are mean ± s.e.m., n = 11-12 independent replicates. e) Pre-treatment of hCMEC/D3 cell monolayers with the MMP2 inhibitor ARP 100 (12 nM, 15 min) prevents the increase in paracellular permeability to a 70 kDa FITC-dextran conjugate induced by pCS stimulation (10 μM, 24 h); data are mean ± s.e.m., n = 6 independent experiments. f) Pre-treatment of hCMEC/D3 cell monolayers with ARP 100 (12 nM, 15 min) prevents the reduction in TEER induced by pCS stimulation (10 μM, 24 h); data are mean ± s.e.m., n = 6 independent experiments. g) Confocal microscopic analysis of expression of the tight junction component zona occludens-1 (ZO-1; white) in hCMEC/D3 cells following treatment with either pCS (10 μM, 24 h), ARP 100 (12 nM, 24 h) or both (ARP 100 12 nM, 15 min pre-treatment, followed by pCS 10 μM, 24 h); nuclei are counterstained with DAPI (blue), scale = 15 μm . Images are representative of at least three independent experiments. h) Pre-treatment of hCMEC/D3 cell monolayers with the MMP9 inhibitor JNJ0966 (440 nM, 15 min) prevents the increase in paracellular permeability to a 70 kDa FITC-dextran conjugate induced by pCS stimulation (10 μM, 24 h); data are mean ± s.e.m., n = 6 independent experiments. i) Pre-treatment of hCMEC/D3 cell monolayers with JNJ0966 (440 nM, 15 min) prevents the reduction in TEER induced by pCS stimulation (10 μM, 24 h); data are mean ± s.e.m., n = 6 independent experiments. j) Confocal microscopic analysis of expression of the tight junction component zona occludens-1 (ZO-1; white) in hCMEC/D3 cells following treatment with either pCS (10 μM, 24 h), JNJ0966 (440 nM, 24 h) or both (JNJ0966 440 nM, 15 min pre-treatment, followed by pCS 10 μM, 24 h); nuclei are counterstained with DAPI (blue), scale = 15 μm. Images are representative of at least three independent experiments.

Figure 6: Treatment with pCS induces BBB permeability *in vivo* through EGFR-dependent mobilisation of MMP2 and MMP9. a) Increased extravasation of Evans blue tracer into the parenchyma of male C57Bl/6 mice following i.p. injection of pCS (10 mg/kg, 2 h exposure) is prevented by erlotinib administration (50 mg/kg i.p., 1 h pre-treatment); data are mean ± s.e.m., n = 5-6 animals. b) Increased extravasation of Evans blue tracer into the parenchyma of male C57Bl/6 mice following i.p. injection of pCS (10 mg/kg, 2 h exposure) is prevented by administration of the dual-specific MMP2/MMP9 inhibitor SB-3CT (10 mg/kg i.p., 1 h pre-treatment); data are mean ± s.e.m., n = 5-6 animals. c) Typical immunohistochemical analysis of MMP2 and MMP9 expression within the cerebral microvasculature of male C57Bl/6 mice treated with pCS (10 mg/kg, i.p. 2 h) with or without erlotinib pre-treatment (50 mg/kg, i.p. 1 h pre-treatment); nuclei are counterstained with haematoxylin, scale bar = 10 μm. d) Typical expression of ZO-1 (white) within the cerebral microvasculature of male C57Bl/6 mice treated with pCS (10 mg/kg, i.p. 2 h) with or without erlotinib pre-treatment (50 mg/kg, i.p. 1 h pre-treatment); nuclei are counterstained with DAPI (blue), scale bar = 10 μm.

Figure 7: Sera from human haemodialysis patients significantly enhances endothelial permeability, an effect prevented by erlotinib pre-treatment. a) Treatment of hCMEC/D3 monolayers with medium containing de-complemented sera from patients undergoing haemodialysis (20 %, 24 h) significantly enhances permeability to a 70 kDa FITC-dextran tracer, an effect not seen with equivalent sera from healthy donors, and prevented by inclusion of erlotinib (2.5 μM, 10 min); data are mean ± s.e.m., n = 10-11 donors. b) TEER of hCMEC/D3 monolayers is not affected by treatment with media containing sera (20 %, 24 h) from either haemodialysis patients or healthy donors, nor by erlotinib inclusion (2.5 μM, 10 min pre-treatment); data are mean ± s.e.m., n = 10-11 donors. c) Treatment of hCMEC/D3 cells with medium containing de-complemented sera (20 %, 24 h) from patients undergoing haemodialysis, but not with that from healthy donors, increases expression of MMP2; data are mean ± s.e.m., n = 10-11 donors. d) Treatment of hCMEC/D3 cells with medium containing de-complemented sera (20 %, 24 h) from patients undergoing haemodialysis, but not with that from healthy donors, increases expression of MMP9; data are mean ± s.e.m., n = 10-11 donors. e) Correlation between concentrations of pCS in human sera samples (healthy donors in black, haemodialysis patients in red) with 70 kDa FITC-dextran permeability data from (a) above; n = 10-11 donors. f) Correlation between concentrations of xanthurenic acid in human sera samples (healthy donors in black, haemodialysis patients in red) with 70 kDa FITC-dextran permeability data from (a) above; n = 10-11 donors.

Table 1: Significant results generated from SPIA of 380 significantly differentially expressed genes.

Name	KEGG pathway ID	pGFdr	pGFWER	Status
Glutamatergic synapse	mmu:04724	2.83×10^{-4}	2.83×10^{-4}	Inhibited
Circadian entrainment	mmu:04713	2.98×10^{-3}	5.97×10^{-3}	Inhibited
Alzheimer disease	mmu:05010	1.40×10^{-2}	4.20×10^{-2}	Inhibited
Amphetamine addiction	mmu:05031	1.92×10^{-2}	7.68×10^{-2}	Inhibited
Oxytocin signalling pathway	mmu:04921	2.54×10^{-2}	1.27×10^{-1}	Inhibited
Glucagon Signaling pathway	mmu:04922	2.75×10^{-2}	1.72×10^{-1}	Inhibited
Retrograde endocannabinoid signalling	mmu:04723	2.75×10^{-2}	1.92×10^{-1}	Inhibited
Pathways of neurodegeneration - multiple diseases	mmu:05022	2.98×10^{-2}	2.66×10^{-1}	Inhibited
VEGF signalling pathway	mmu:04370	2.98×10^{-2}	2.68×10^{-1}	Inhibited
Cellular senescence	mmu:04218	3.12×10^{-2}	3.13×10^{-1}	Inhibited
Aldosterone synthesis and secretion	mmu:04925	3.12×10^{-2}	3.43×10^{-1}	Inhibited
Ras signalling pathway	mmu:04014	4.14×10^{-2}	4.96×10^{-1}	Inhibited
C-type lectin receptor signalling pathway	mmu:04625	4.18×10^{-2}	5.44×10^{-1}	Inhibited
Coronavirus disease - COVID-19	mmu:05171	4.59×10^{-2}	6.42×10^{-1}	Activated
Lipid and atherosclerosis	mmu:05417	4.83×10^{-2}	7.24×10^{-1}	Inhibited
Gastric acid secretion	mmu:04971	4.94×10^{-2}	7.90×10^{-1}	Inhibited
Huntington disease	mmu:05016	4.97×10^{-2}	8.45×10^{-1}	Inhibited

Table 2: Serum donor demographics.

	Age (years)	Sex ratio	Serum urea (mg/dl)	Serum creatinine (μM)	Renal replacement therapy duration (years)
Healthy donor	49 ± 3.3	8F : 3M	4.46 ± 0.36	82.0 ± 6.8	N/A
Haemodialysis	59 ± 6.2	4F : 6M	19.13 ± 1.90	876.2 ± 94.7	10.6 ± 4.2

Table 3: Serum metabolite concentrations. LC-MS/MS determined concentrations of different potential uraemic toxins in sera from healthy donors and individuals undergoing haemodialysis for nephropathy, alongside coefficients of correlation between metabolite concentration and permeability of hCMEC/D3 cells to a 70 kDa FITC-dextran tracer following treatment with 20% sera for 24 h; n = 10-11, * P<0.05 *vs.* healthy donors.

Metabolite	**Healthy donor (µM)**	**Haemodialysis (µM)**	**Permeability correlation**	
			Rho	**P_{FDR}**
p-Cresol sulfate	14.12 ± 3.09	155.26 ± 27.36 *	0.675	0.01
p-Cresol glucuronide	0.09 ± 0.03	10.63 ± 4.44 *	0.394	0.12
Indoxyl sulfate	2.92 ± 0.45	147.18 ± 26.46 *	0.400	0.09
Serotonin	0.64 ± 0.12	0.42 ± 0.18	-0.233	0.64
Kynurenine	1.73 ± 0.23	4.63 ± 0.57 *	0.371	0.06
3-Hydroxyanthranilic acid	0.01 ± 0.00	0.05 ± 0.01 *	0.434	0.11
Tryptophan	42.30 ± 1.46	22.97 ± 2.35 *	-0.466	0.06
5-Hydroxyindole acetic acid	0.05 ± 0.01	1.28 ± 0.21 *	0.464	0.08
Xanthurenic acid	0.01 ± 0.00	0.17 ± 0.05 *	0.442	0.02
Anthranilic acid	0.20 ± 0.02	0.52 ± 0.1 *	0.396	0.12
Kynurenic acid	0.06 ± 0.01	2.34 ± 0.58 *	0.353	0.16
Indole-3-lactic acid	0.78 ± 0.12	2.42 ± 0.33 *	0.397	0.12
Indole-3-carboxaldehyde	0.05 ± 0.00	0.06 ± 0.01	-0.08	0.78
Indole-carboxylic acid	0.04 ± 0.01	0.06 ± 0.01	0.041	0.89
Indole-3-acetic acid	2.45 ± 0.75	6.36 ± 2.07	0.385	0.17
Indole-3-propionic acid	1.73 ± 0.4	1.37 ± 0.35	0.051	0.47
Methyl indole 3-acetate	0.05 ± 0.03	7.44 ± 3.48 *	0.241	0.43

Figure 1

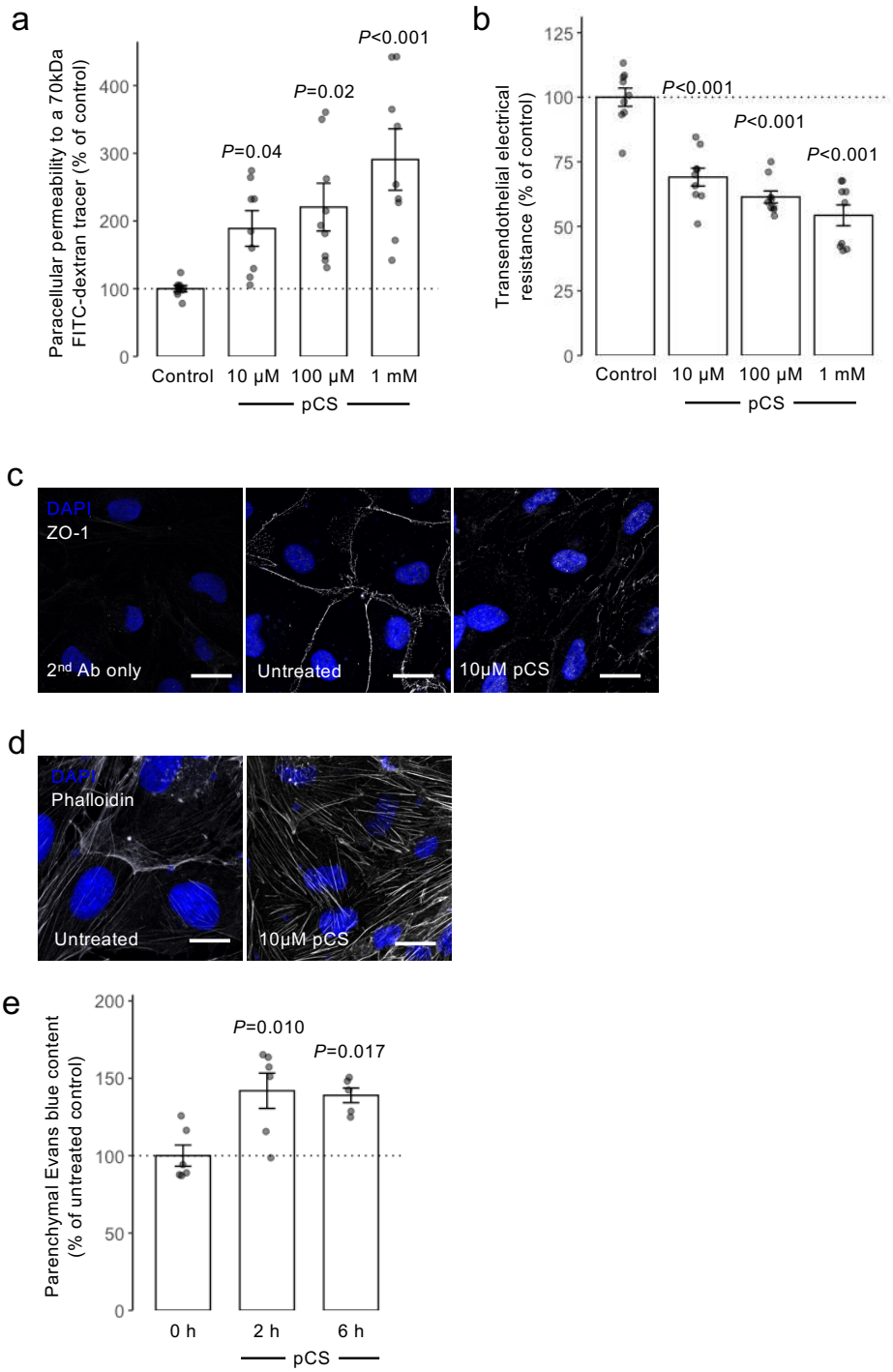

Figure 2

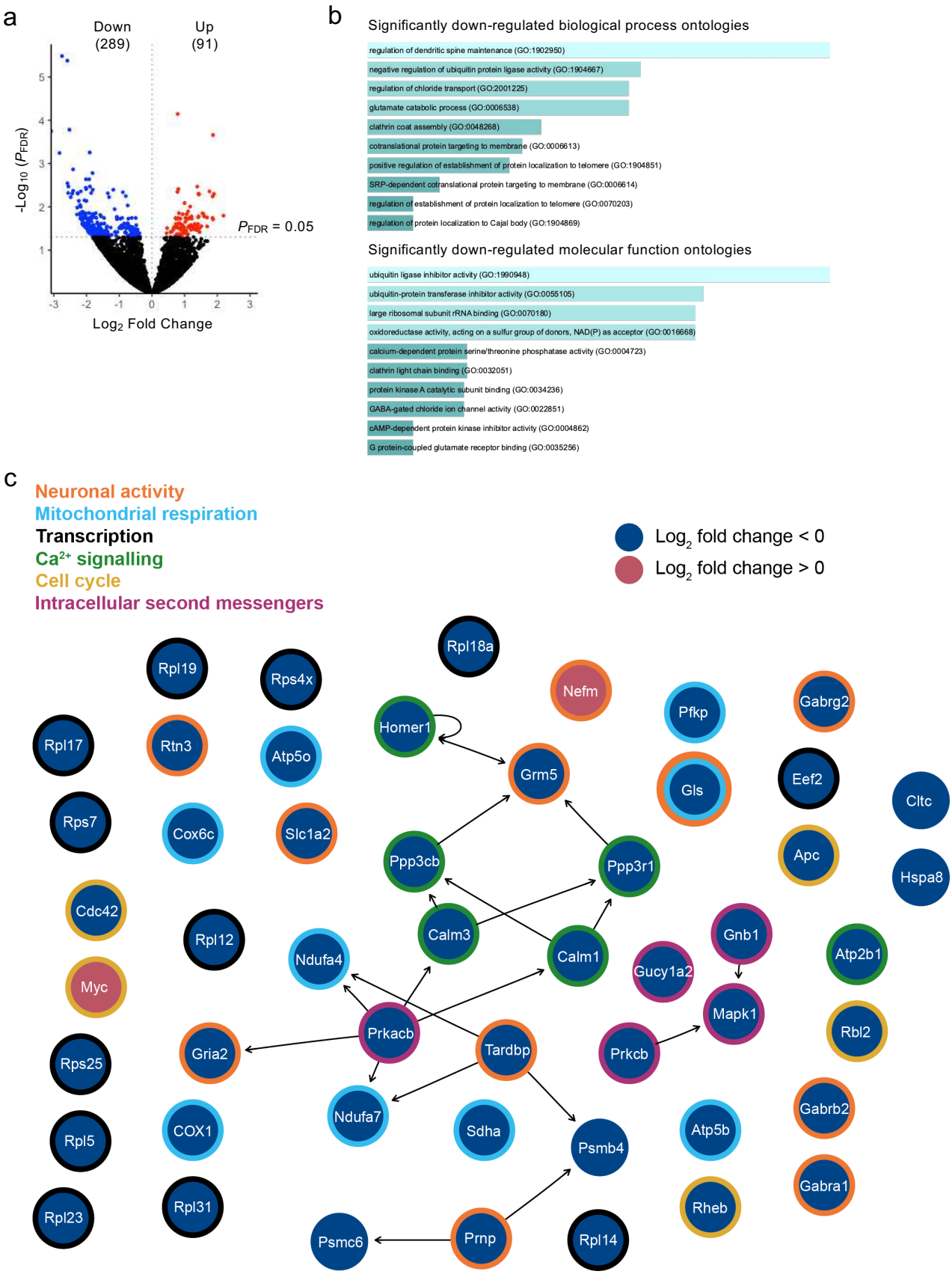

Figure 3

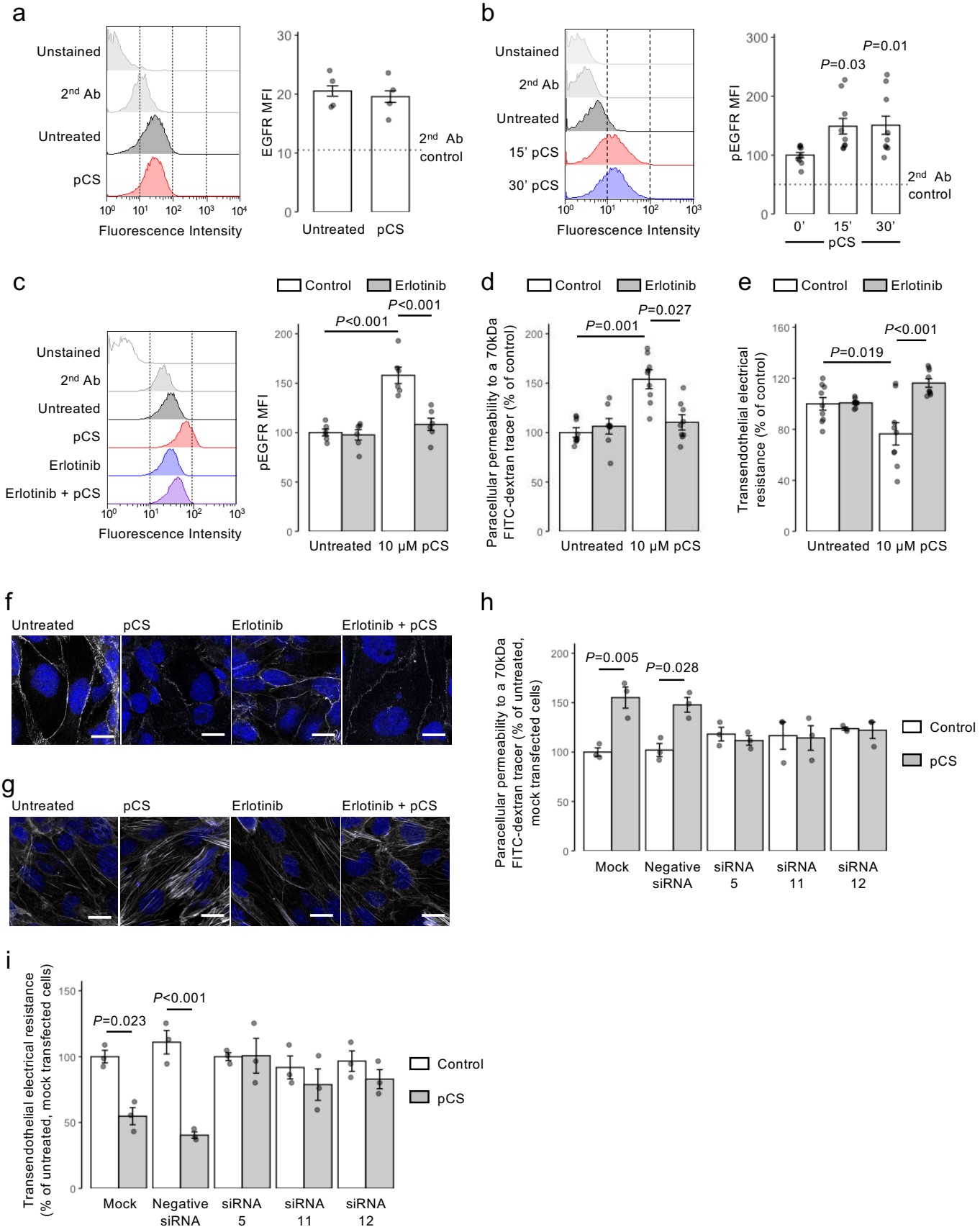

Figure 4

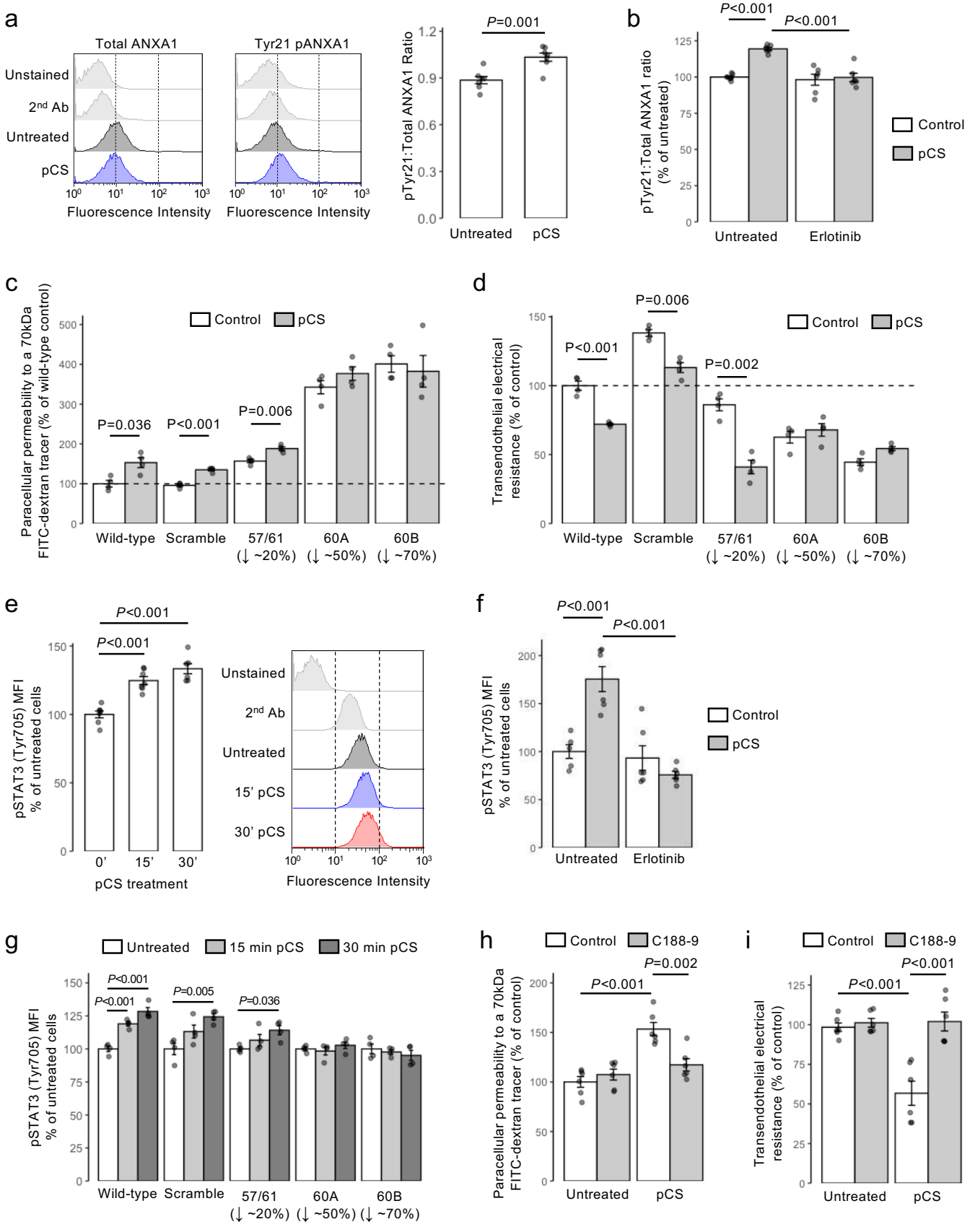

Figure 5

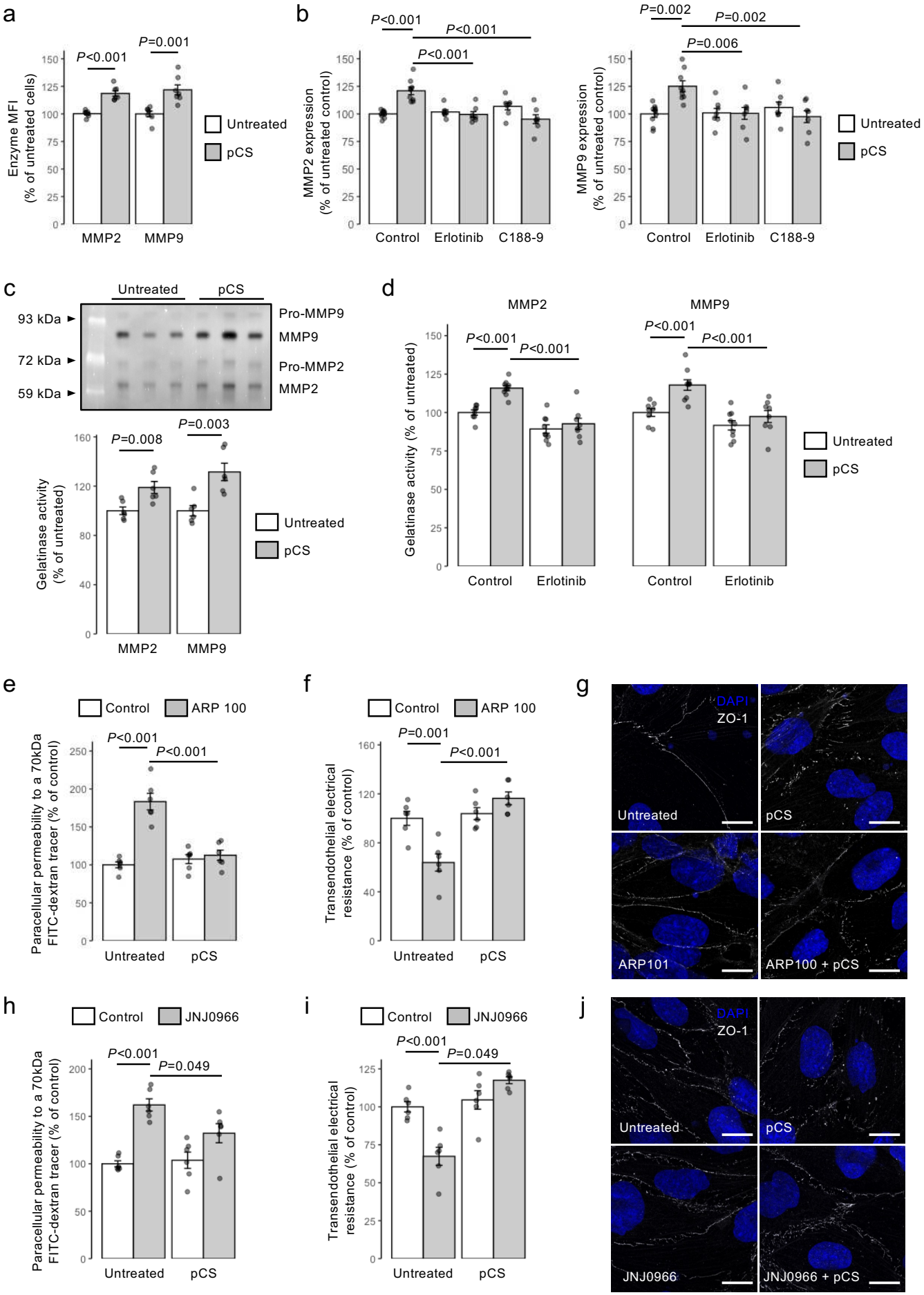

Figure 6

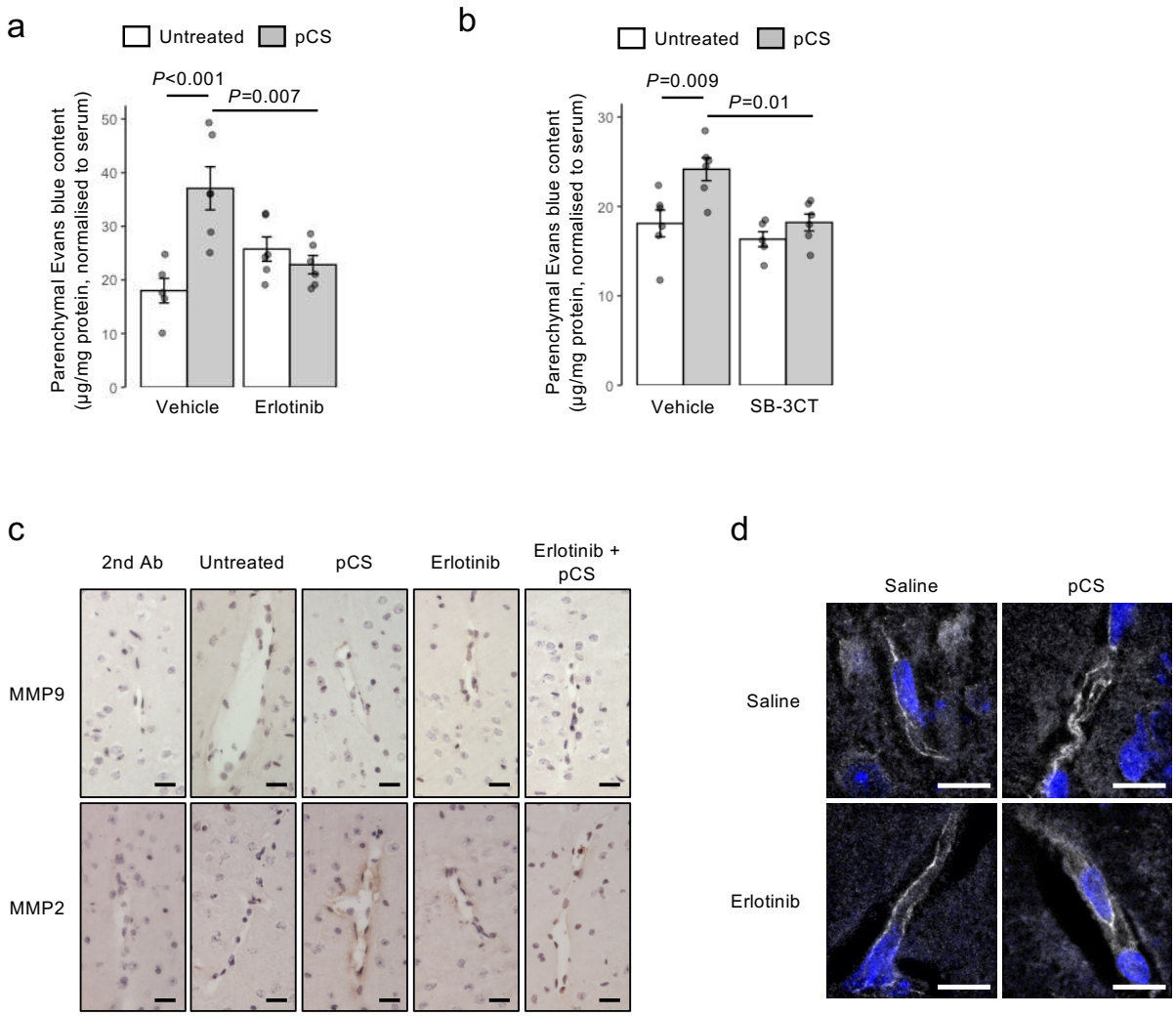

Figure 7